

Internship M1 report

Sediment dynamics and carbon accumulation rates in the subtidal zone: an example of an open mixed tide and wave estuary in the Antioche Strait

Author: Joseph Fournier

Internship supervisors: Benjamin Amann

Abstract:

Subtidal estuarine environments play a crucial yet underexplored role in long-term carbon sequestration. This study investigates sediment and organic carbon accumulation rates (CAR) in the Antioche Strait, a dynamic open mixed tide and wave-dominated estuary in southwestern France. Using a combination of historical bathymetric surveys (1824, 1960, 2022), sediment coring, and organic carbon analysis (via LOI-based TOC estimation), spatial and temporal patterns of sediment accumulation rate (SAR) and CAR were assessed. Results show a significant decline in SAR and CAR over time, from high values between 1824 and 1960 (average CAR: $210 \text{ gC}\cdot\text{m}^{-2}\cdot\text{yr}^{-1}$) to much lower or even negative values in the recent period 1960–2022 (average CAR: $83 \text{ gC}\cdot\text{m}^{-2}\cdot\text{yr}^{-1}$), indicating potential erosion of carbon stocks. High spatial variability is observed, with northern sites displaying the greatest CAR. Testing external forcings such as current speed, proximity to sediment sources, and influence of sediment dumping zones revealed no significant statistical correlation with the spatial distribution of carbon accumulation rates. This lack of correlation underscores the complexity of carbon dynamics in subtidal systems, where multiple interacting factors may obscure clear trends. Nevertheless, the observed values and patterns are consistent with those reported in the global literature, reinforcing the relevance of subtidal estuarine environments as meaningful, yet spatially heterogeneous, contributors to coastal carbon sequestration.

Key words: Blue carbon, subtidal environment, carbon accumulation rate (CAR), Antioche Strait, sediment accumulation rate (SAR)

Acknowledgments:

I would like to thank Benjamin Amann for his valuable guidance and the trust he placed in me. Thanks to Eric Chaumillon for the discussion and for giving me access to Nicolas Weber work. Thanks to Bénédicte Dubillot for laboratory inquiries when Benjamin Amann wasn't here. And finally I would like to thank coworkers of the LIENSs which welcomed me with open arms.

1. Introduction:

Deltaic environments are characterized by very high rates of sediment accumulation and are the gateway by which much of the world's terrigenous organic matter is delivered to the marine environment (García-García et al., 2006; Wilkinson et al., 2018). As sediment accumulation zones, they are preferential areas for organic carbon accumulation and participate, in the same way as terrestrial (e.g. forest) or coastal (e.g. blue carbon ecosystem) ecosystems, to long-term carbon storage. Just as forests sequester carbon in their above-ground biomass, coastal systems sequester carbon in the subterranean layers. So a good carbon sink is first and foremost a sediment sink, where sediment accumulation rates and carbon accumulation rates are intrinsically linked (e.g., in salt marshes; Amann Benjamin et al., 2024). Part of the carbon blue ecosystem, tidal systems and deltas represent $294,956 \pm 30,780 \text{ km}^2$ (Laruelle et al., 2025), it is 3.6 times mangrove surface ($81,849 \text{ km}^2$ in 2012), and it's 5.4 times tidal marshes area ($55,000 \text{ km}^2$) (Macreadie et al., 2019). This makes this ecosystem a significant potential carbon sink. However, subtidal zones are little studied for their carbon sink function. A stepwise keyword-based literature comparison was conducted on Scopus and the results are indisputable: when searching for subtidal and adding one by one carbon and accumulation, the results of the research gives 11050 publications, 640 publications and finally 27 publications (Figure 1). This subtidal estuarine environment is a preferential zone but nevertheless is site-specific and depends on numerous factors such as distance to sediment source (river proximal vs distal, e.g., North Sea, Diesing et al., 2021), wave and tide characteristics, current strength and direction, the bedrock nature, the sediment supply, anthropogenic influence or climate parameters. This, together with a high spatial variability in carbon content and SAR, imply a wide range of carbon accumulation rates reported for these environment This leads to carbon accumulation rates (CAR) that vary greatly in subtidal/coastal shelf areas from 7 to 1600 $\text{gC/m}^2/\text{yr}$, with a median of 19.6 $\text{gC/m}^2/\text{yr}$ (Wilkinson et al., 2018, REVIEW, n=26). In the present work, the spatial distribution of SAR and CAR in the subtidal area of the Antioche Strait (SW France), an open mixed tide and wave estuary, is evaluated. For this purpose, volumetric and rates of sediment accumulation have been estimated by differencing bathymetric surveys taken at different times. Then carbon content (TOC) has been measured on sediment cores, sampled previously during the year by the M1 GGL class (La Rochelle University). From SAR and TOC, CARs have been computed. And finally, according to these results, influence of external parameters such as distance to river mouth, direction and strength of currents, and the potential influence of the pilling zone on SAR and CAR in the Antioche Strait, have been questioned. A better understanding carbon stocks and accumulation rates will contribute to "La Rochelle Territoire Zero Carbon" project and its ambition towards carbon neutrality by 2040

2. General setting:

The Antioche Strait is a 10 km-wide and 40 km-long open, mixed tide and wave estuary located on the passive continental margin of the Bay of Biscay, near La Rochelle. It originates from the infilling of the incised Charente valley, developed on a stable, rocky, and sediment-deprived margin (Weber et al., 2004; Schmitt and Chaumillon, 2023). The tidal regime is semidiurnal with slight diurnal asymmetry, and a coastal tidal range varying from ~1 m during neap tides to >6.5 m during spring tides, averaging 3.75 m annually in La Rochelle Harbour (Schmitt and Chaumillon, 2023). The Charente estuary is hypersynchronous, meaning an increasing tidal range within the estuary (Toublanc et al., 2015). Swells predominantly from the W-NW (56%) reach an average significant wave height of 1.5 m and periods of 6–12 s. Storm waves regularly exceed 6 m, with ~60 storm events recorded since 1924 (Breilh et al., 2014; Schmitt and Chaumillon, 2023). Sediments in the strait are sourced from local rivers (Sèvre Niortaise, Charente, Seudre) and significantly from the Gironde Estuary, contributing up to 85% south of Marennes-Oléron (Poirier et al., 2020). Resuspension of fine particles, mainly driven by wind waves, causes high turbidity during storms (Gouleau et al., n.d.).

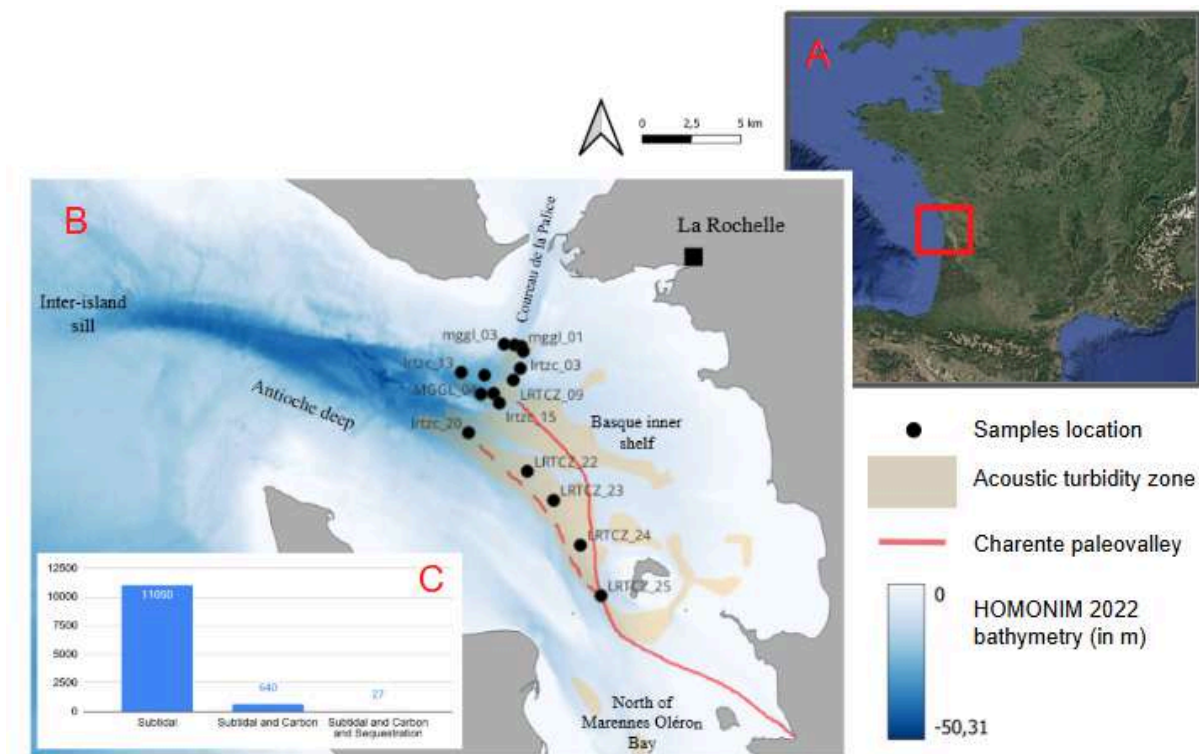


Figure 1: Antioche Strait location (A) and study site characteristics like the Thalweg of the main eastern segment of the Charente paleo-valley (solid line), and of the secondary western segment (dotted line) (B). Scopus stepwise keyword-based literature comparison

The estuary is divided into three sectors: the distal inter-island sill (an erosive zone disconnected from upstream supply), the proximal Basque inner shelf (an accretion zone), and the Antioche deep in between. The study area, located in the inner Antioche zone, is characterized by thick mud drapes overlying a fining-upward architecture, with isopach thicknesses reaching several meters (Weber, 2004, unpublished thesis). These sediments often trap shallow gas, evidenced by strong acoustic backscatter and absorption in seismic profiles (200–10,000 Hz; Weber unpublished). Anaerobic bacterial methanogenesis of buried organic matter are likely responsible for the generation of shallow gas in sediments where sulfate reduction and methane production dominate decomposition (Weber, unpublished)

3. Material and Methods:

3.1. Core sampling and sample preparation

During a 2-day excursion on board of the Côtes de la Manche (IFREMER vessel, semester practical work module: campagne à la mer of Marine geology and oceanography course), 16 sediment short cores and 9 grab samples were retrieved with the uwitec corer and van veen grab, respectively (Appendix 1). Samples were also retrieved in and out the shallow gaz area (acoustic turbidity zone) to see if a difference can be observed in SAR and CAR (Figure 2). Sediment cores of 8 to 27 cm long have been realized and each sediment core was subsampled on board with a 1 cm resolution. Samples were collected in ziploc bags and stored in a cooler and then transferred to a fridge upon arrival to the lab. The 1 cm samples were freeze-dried, then homogenized using a mortar. From the ratio of cuttlefish mass to wet mass, the water content was estimated, providing dry bulk density (DBD) from the volume of sample taken.

3.2. Bathymetric differences and sediment accumulation rates :

Bathymetric data from different years were used to obtain a depth-age control/estimate of the sediment cores and to estimate sediment accumulation rates (SAR, in cm/yr) between each period. The first one used is 1824 bathymetry (SHOM, provided by Poirier et al., 2020), which has a vertical error of 2.6m (Laura's report RTE). Then 1960 bathymetry was used by applying vertical correction of 1.29 m in the data (Laura's report RTE). Finally, the 2022 bathymetry from SHOM was used, with a horizontal resolution ranging from 5 to 20 m (0.00005° – 0.0002°) depending on the zone, and a vertical uncertainty estimated at ~1% of the mesh size (i.e., 0.05 to 0.2 m). QGIS was used to (i) interpolate spatially bathymetric data into a raster using the function Triangulated Irregular Network (TIN) from a point vector layer, and (ii) determine the bathymetric differences and using the raster calculator function for three time periods 1824-2022, 1824-1960, and 1960-2022.

Bathymetric datasets from 1824, 1960, and 2022 were used to assess long-term and intermediate sediment accumulation trends. The 1824 bathymetry was selected for its fine resolution and frequent use as a regional reference (Bertin et al., 2005; Poirier et al., 2020), while the 2022 bathymetry from SHOM (HOMONIM Project) provided the most recent and accurate data. Other intermediate bathymetries exist but were not considered to keep a signal-to-noise ratio sufficiently high to detect significant SAR value (above margins of error)

3.3. Organic matter measurement and organic carbon estimation

0.5g \pm 0.01g of the homogenised parent samples were used to measure organic matter (OM) content using the loss on ignition technique (LOI). For this, the samples were placed in a muffle furnace for 14h at 550°C (Amann et al., 2023; Baustian et al., 2017). OM % is determined by the weight difference before and after LOI. Then, total organic carbon (TOC) content was determined indirectly from OM content by applying the transfer function developed by Amann et al., (2023) using sediment samples from the Pertuis Charentais, following the formula : $TOC = 0.33 * OM - 2.94$ (Appendix 2). This indirect method to quantify organic carbon comes from a linear regression between LOI 550°C during 14h experiment results and direct organic carbon measurement made by a TOC analyser. This correction formula was selected as the samples come from suspended matter, saltmarshes and mudflat of the studied zone.

3.4. Carbon accumulation rate

From the division of dry sample weight by the volume of the sample, a diameter disc the size of the uwitec corer and about 1 cm thick, it was possible to access the dry bulk density (Amann). From it, Carbon accumulation (CAR) was compute as follow : $CAR = SAR * TOC * DBD$ and converted in $gC. m^{-2} y^{-1}$.

3.5. Forcing variables

Several external variables were tested for their potential influence on CAR variability. First, the distance from the Charente River mouth (arbitrarily set at lon=384393, lat=6547571; ESPG:2154) was considered as a proxy for sediment supply. We also analyzed average coastal inorganic suspended particle concentrations (SPM-R, in $g \cdot m^{-3}$) from ocean color data (Aqua MODIS) for the period 2016–2021 (Amann et al., 2024; Novoa et al., 2017). Historical bathymetry from 1675 (Poirier et al., 2020), expressed in “pied du Roy” (1 pdR = 0.242 m), was used to estimate available accommodation space over time. Hydrodynamic forcing was assessed using TELEMAC-2D current model outputs (EDF, SHOM) for spring and neap tides (range 45 and 95), from -6 to +6 h relative to low tide in La Rochelle. Current vectors were computed from zonal and meridional components (in tenths of knots) and averaged per sample using the three nearest nodes weighted by inverse distance. Lastly, the proximity to the Lavardin offshore dumping zone (1 km diameter, centered at lon = 372880, lat = 6567871; ESPG:2154) was evaluated, where 340,000–360,000 m³ of dredged

sediments were deposited annually (2020–2021) from nearby ports and the Port Horizon 2025 project. Pearson correlation tests ($p < 0.05$) were conducted between CAR and all external variables using Python.

4. Results:

4.1. Sediment accumulation rates

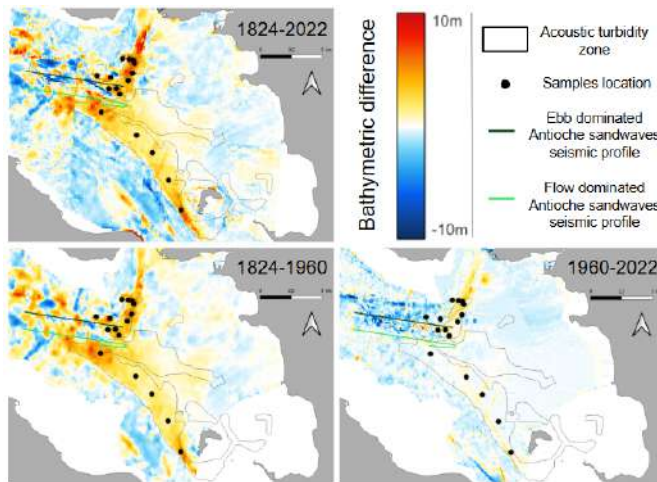


Figure 2: Bathymetric differences of the Rade des basques during different periods. The gradient of color is chosen according to the 1824-2022 periods which range from 10 to -10 meters but do not represent the extreme value that can be greater than that one. The seismic profile corresponds to the profile followed during the sea trip to study the asymmetry of the Antioche sandwaves.

The bathymetric difference with the longest period (1824-2022) shows generalized accretion on this long-term with values from -16 to 10m (which is . The Rade des Basques accretion, with maximum value located within the northern acoustic turbidity zone, corresponds to Charente paleochannels and trough, where the tidal prism is greater and where sedimentation is favored (Figure 2A). Erosional surfaces are less widespread and are weak along the Rade des Basques mudflat (-5m) but are higher in the Atioche deep (-16m). The intermediate bathymetric difference between 1824 and 1960 shows similar accretion trends between 1824 and 2022, but with lower values, respectively +6m, -1m and -7m, compared with the areas tested previously.

Table 1: Sediment accumulation rate, inside (black) and outside (red) the error margin, in function of the period. The errors are respectively 1.36, 3.01 and 2.58 cm/yr. The sample IDs are sorting from the northernmost to the southernmost point. The grey bars highlight the core samples used for TOC content in this study.

Sample ID	SAR 1824-2022 (in cm/yr)	SAR 1824-1960 (in cm/yr)	SAR 1960-2022 (in cm/yr)
mggl_03	1.51	2.4	-0.45
mggl_02	1.85	0.99	3.72
mggl_01	4.46	4.89	3.54
lrtc_03	3.98	4.51	2.82
lrtc_04	1.97	2.26	1.32
lrtc_13	0.81	2.3	-2.46
MGGL_04	1.20	3.15	-3.07
LRTC_09	2.54	3.51	0.42
MGGL_05	2.37	2.68	1.7
lrtc_14	1.56	1.26	2.22
lrtc_15	2.22	3.07	0.34
lrtc_20	1.91	2.87	-0.22
LRTC_22	1.19	2.14	-0.89
LRTC_23	1.10	1.52	0.16
LRTC_24	0.89	1.38	-0.19
LRTC_25	2.46	3.33	0.57

On the other hand, the most recent period (1960-2022) shows much smaller bathymetric differences, with only accretion to the north, and areas of little variation (white within the margin of error, ± 1.6 m) or even generalized erosion in the other areas.

From these differences of bathymetry, sediment accumulation rates (SAR in cm/yr) were extracted from each point and the three periods (1824-2022; 1824-1960; 1960-2022; Table 1). The generalized accretion 1824-2022 is strongly influenced by 1824-1960 bathymetric difference. SAR range from -3.07 to 4.89

4.2. Sediment organic carbon

Total organic carbon (TOC) data range from -0.57 and 2.97 % (Figure 3; Supplementary 1). Remarks: negative values in TOC are due to the calibration function used to indirectly estimate TOC from the loss-on-ignition technique (Amann et al., 2023), which does not seem to be adapted for low organic matter content. This calibration function will be refined post master work through the analysis of sediment organic carbon content by an elemental analyzer.

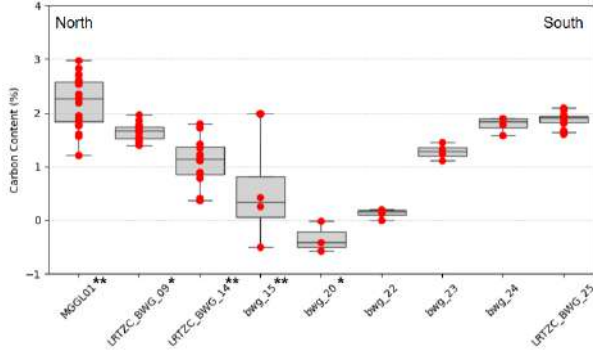


Figure 3: Total organic carbon distribution in function of the core samples. The simple asterisk represents a standard deviation superior or equal to 0.15 and the double asterisk indicates a standard deviation superior to 0.30.

For half of the sample, the southernmost one, the distribution of the carbon content is very tight and might only correspond to the experiment error associated with the LOI technique. However, TOC of the half northernmost points vary in a more significant way, represented by an asterisk and to a greater extent the result followed by a double one. The sample bwg_20, among others, displays a negative TOC which is not possible. In fact, its LOI values were too small and thus the Amann correction gives negative results. By using the same methodology for each of the samples, the relative differences are real, negative TOC values will be considered equal to 0%.

Interestingly, TOC decreases from north to south (2.94 to 0%), until bwg_20, before increasing again up to 2%. For these samples, TOC increases according to a west-east gradient. All the TOC values are below 2% except for the point MGGL01, which displays a mean TOC value of 2.20%, with values ranging from 1.21 to 2.97%. It can also be noted that all samples located towards the southern region (from BWG20 to BWG25) present a lower TOC variability than samples located in the northern zone.

4.3. Carbon accumulation rates

4.3.1. Temporal and spatial variability

Carbon accumulation rates (CAR) were computed from DBD data ranging from 0.38 and 1.05 g.cm^{-3} and the previous TOC results. CAR ranges from -19 to $640 \text{ gC.m}^{-2} \text{ y}^{-1}$, with systematically higher values during the initial period 1824-1960 compared to the most recent period 1960-2022 (Table 2).

Negative values are further found in recent times corresponding to an erosion of the carbon stocks. The full period 1824-2022 thus presents intermediate CAR values. This is true for each individual value and for the average CAR with: $210 \pm 206 \text{ gC.m}^{-2} \text{ y}^{-1}$ for the period 1824-1960, $83 \pm 155 \text{ gC.m}^{-2} \text{ y}^{-1}$ for 1960-2020, and $170 \pm 181 \text{ gC.m}^{-2} \text{ y}^{-1}$ for the full period 1824-2022. This trend follows closely the sediment

Table 2: Mean carbon accumulation rates of the different core samples for the different time-periods. The positive values (black) refer to sediment accumulation, while the negative one (blue) refer to sediment erosion derived from the analysis in bathymetry differences. STD stands for mean standard deviation and IQR stands for interquartile range and is computed as follow: $Q3-Q1$

Sample_id	CAR [$\text{gC.m}^{-2} \text{ y}^{-1}$]		
	1824-2022	1824-1960	1960-2022
MGGL01	585.1	640.3	463.9
LRTZC_BWG_09	284.7	393.1	46.7
LRTZC_BWG_14	126.1	101.9	179.0
LRTZC_BWG_15	97.7	135.4	15.2
lrtzc_bwg_20	0.0	0.0	0.0
LRTZC_BWG_22	13.6	24.5	-10.2
LRTZC_BWG_23	88.7	138.0	-19.2
LRTZC_BWG_24	97.1	135.1	13.9
LRTZC_BWG_25	239.8	323.6	55.9
Average	170.3	210.2	82.8

accumulation rates, as expressed by the high correlation between the two variables ($r_{av} = 0.92, p=0.0006 < 0.05$; Table 3).

STD	181.2	205.6	154.8
Median	97.7	135.4	15.2
IQR	151.0	221.6	55.9

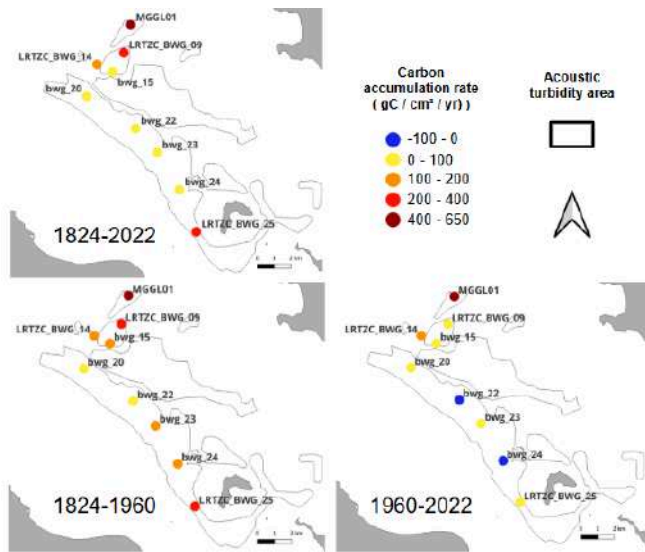


Figure 4: Carbon accumulation rates in the Antioche strait according to the three periods.

Spatially, whatever the period considered, CAR values are generally greater for the northern zone than for the south with the exception of the southernmost sample BWG15 that presents high CAR comparable to the north zone (Figure 4). Punctually, MGGL01 presents the maximal CAR values disregarding the period considered (640

$gC.m^{-2}.y^{-1}$ and $464 gC.m^{-2}.y^{-1}$ for the period 1824-1960 and 1960-2022, respectively). No relation could be found between CAR values and the presence/absence of the acoustic turbidity zones.

4.3.2. Correlation between CAR, and SAR and TOC

Correlation tests obtained from the different variables show that CAR values are highly correlated ($p < 0.05$) to both SAR and TOC content for all considered time periods. The only exception occurs for the correlation non significant between CAR and TOC for the period 1824-2022. This shows that both SAR and TOC are important parameters influencing CAR variability in the Antioche Strait.

Table 3: Pearson correlation coefficients (r) and two-tailed p -values ($n = 9$), based on the t -distribution.

Periods	Correlation (CAR, SAR)	P-value	Correlation (CAR, TOC)	P-value
1824-2022	0.95	0.0001	0.56	0.1178
1824-1960	0.88	0.0015	0.81	0.0076
1960-2022	0.94	0.0002	0.78	0.0134

4.4. Forcing factors

Pearson correlation tests first show that CAR values are positively and significantly ($p < 0.05$) correlated for all three periods, which indicates that the spatial pattern is preserved through the three periods (Figure 5). However, speed currents are for all CAR anti-correlated, even though non significant, probably due to the difference of the north and south samples. CAR and suspended matter are positively correlated, but not significantly (p -value > 0.05)

.Surprisingly, CAR values increase with distance from the Charente River mouth for the southern points (BGW_25, 24, 23, 22, 20; refer to figure CAR), there is no significant correlation ($p>0.05$) between CAR and distance to the river mouth. This is likely due to high CAR values found in the northern distal zone. On the contrary, CAR and distance to the Lavardin dumping zone are anti-correlated, with no significant correlation besides high CAR values in the north, which means that CAR decreases when moving away from the offshore dumping zone.

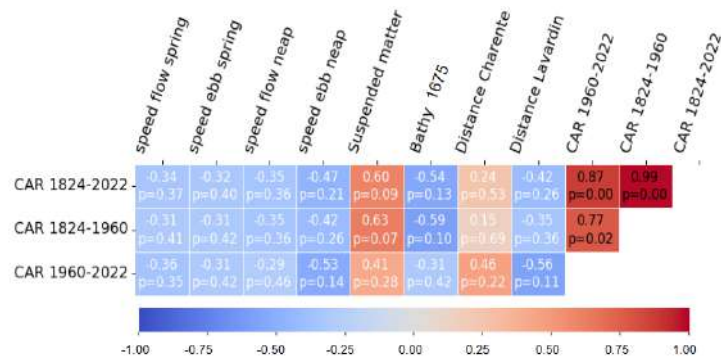


Figure 5: Pearson correlation matrix between carbon accumulation rates and external factors such as, the speed of the current (in tenths of knots) and its direction (in degrees with trigonometric rotation East = 0°), the distance to the Charente River mouth (in km), the concentration of suspended matter (in $g \cdot m^{-3}$; SPM-R, Aqua MODIS), and the bathymetry of 1670 (in pdr)

5. Discussion:

5.1. Bathymetric differences and sediment accumulation rates

Results from the bathymetric-difference approach show that the sedimentation accumulation is not linear over the time. There are few hypotheses to explain the slow down of accretion observed during the last sub-period compare to the 1824-1960 large accretion period, which could be: (1) a decrease in sediment supplies (REF), and (2) changes in hydrology induced by climatic trends. Previous regional studies have shown the combined influence of land clearance and increase in catchment rainfall on sediment accretion over the 18th century (Poirier et al., 2011). This could explain high SAR for the early period, while monitoring of discharge in the main coastal river in France reported a 20 to 30% decrease over the last 50 years, which could be associated with a decrease in sediment supply over time (BRGM (direction), 2020). Another hypothesis is: (3) a stagnation of eustatic level and sediment filling of the area, reducing the tidal prism and free space

Nevertheless, interpreting depth changes over time is challenging due to the cumulative nature of vertical (Z) errors associated with each bathymetric dataset. When calculating bathymetric differences, the total uncertainty corresponds to the sum of the vertical errors from both time steps. Consequently, the shorter the time interval considered, the more difficult it becomes to distinguish real sedimentation or erosion signals from noise within the error margins. This is particularly critical when accretion rates are low. Despite improvements in measurement resolution and instrument accuracy over time, shorter periods such as the most recent one (1960–2022, 62 years) remain more affected by relative uncertainty. In that period, lower accretion rates often fall within or close to the vertical error threshold, making the detection and quantification of sediment accumulation less robust. Indeed, 67% of the SAR values are significant for the 1824-2022 period, 44% for 1824-1960 period, and only 11% for 1960-2022 period (Table 1).

Classically, sediment accumulation rates are obtained by dating sediment cores using the radioisotope ^{210}Pb (García-García et al., 2006; Diesing et al., 2021), but this technique is time-consuming (~24h/sample). ^{210}Pb analysis is planned as an outlook to this two-month work and will be used to strengthen SAR obtained by the multiple-bathymetry approach.

The acoustic turbidity zone boundaries are well associated with high sedimentation rates in early times as pointed out by the bathymetric differences based on the 1824 bathymetry (Figure 2). However, since 1960, low sediment accumulation and even erosion have been found in these zones. This can induce a degradation of surface sediment layers, making it more vulnerable to gas pressure, ultimately favoring gas liberation. This has important implications with what concerns the carbon budget of this subtidal zone, and the importance to associate measurements at the sediment-water-air interface (C captation/emission). Studies addressing this second point are currently underway in the Pertuis d'Antioche (LIENSs, LRU).

5.2. Organic carbon content

This part of the discussion will approach the TOC values distribution dichotomy first between the north and the south (Figure 3). In particular, TOC values tend to decrease with increasing distance from the sediment source. This is the case for the southeast-west transect where TOC decreases with distance from the mouth of the Charente. For the northern part the relationship between distance from the sediment source and lower TOC values is less obvious.

Sediment could come from the Breton Strait, located at the north of the Ré island that connects to the Antioche Strait by the Coureau de la Palice, and driven by ebb current (Figure 6). Sediment originating from the Lavardin offshore dumping zone can also greatly impact TOC content in the samples (Figure 6).

As it stands, results from this study cannot unravel the contribution of these different sources. Nevertheless, the next step in my internship will be to analyse the isotopic signature of organic carbon $\delta^{13}C$, to determine the sedimentary source of the sediment samples. It will be tested whether it is possible to distinguish the contribution from marine ($\delta^{13}C$ around -18 to -23‰) vs. terrestrial ($\delta^{13}C$ closer to -31‰) input and potentially the contribution of dragged sediments to the sampling sites.

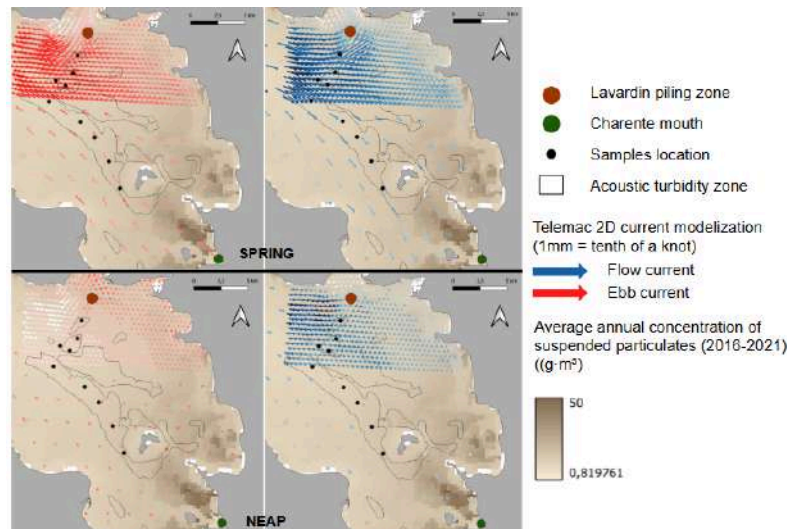


Figure 5: Maps showing the direction and strength of the current (blue arrows for the flow, red arrows for Ebb currents) during spring tide (above two panels) and neap tide conditions (lower two panels). The coloured background refers to the concentration of suspended matter in the coastal waters (brown gradient). The zone of the Lavardin piling and the Charente River mouth are also placed on this figure.

Another potential factor influencing the TOC values is the sand supply. In particular, the Antioche deep in the West (-40m water depth) is characterized by asymmetrical sand dunes (2-9m amplitude, 500-200m wavelength) that tend to migrate according to the currents, with crests migration of 30 to 40 m reported (10 to 13 m/year) (Weber and Chaumillon, n.d.; Fournier & Tephany, unpublished). This sandwave migration could potentially explain lower TOC content in the westernmost samples (e.g., BWG20, BWG14). Although no significant proportion of sand could be found in any sediment samples, grain-size analysis could provide very supportive information in this context.

Wind waves regime could also help explain the W-E gradient in the south, an important parameter for sediment resuspension. Exploring the regimes of waves and wind regimes will be necessary beyond this two-month work to better understand CAR variability in this open mixed tide and wave estuary.

TOC data also revealed the limits of using indirect carbon quantification from the literature. Although TOC values are within the range of those found in lower sections of cores from mudflat and saltmarsh, the calibration function developed by Amann et al., (2023) does not apply for LOI lower than 8.9%. This limitation justifies the use of organic carbon analyser in order to have the precise value of carbon and therefore utilising a more precise calibration curve; this is to be undertaken at the end of June.

5.3. Carbon accumulation rates

CAR was shown to be highly correlated both with SAR and TOC variability (Table 3). This suggests that both sediment accumulation rates and the amount of organic carbon in sediment are important parameters explaining the CAR variability. As such, the spatial CAR variability follows the V shape spatially found for TOC with higher CAR found for the northernmost sample (BWG01) and south-easternmost sample (BWG25), and the lowest values towards the South-West (e.g., BWG20) (Figure 4). Similarly, CAR values follow the spatio-temporal variability of SAR, with the highest values found for the first period investigated 1824-1960, and lowest in the most recent 1960-2022 with negative CAR (erosion) values reported in the south.

The correlation tests operated between CAR and external parameters (flow and ebb speed, suspended matter concentration, distance from the Charente River mouth, distance from the Lavardin sediment source, and free space from 1670) revealed that all parameters failed to explain the spatial CAR variability. All correlations are non significant ($p > 0.05$). The fact that neither correlation nor anti-correlation have been significantly established shows the complexity of spatial CAR, which might be influenced by multiple factors simultaneously and not in the same proportions everywhere.

This lack of correlation could also be due to the influence of the two high CAR zones located at the extremity of our studied site close to the Lavardin (MGGL01) and the Charente River mouth (BWG25) respectively. For testing these parameters, it would have been better and geographically relevant, to subdivide CAR into south and north groups and run the correlation test again (except maybe for offshore dumping zone - south group and charente mouth - north group). In particular, the northernmost point (MGGL01) presents significantly higher CAR than all other points, which seems to drive the correlation statistics. It would be interesting to test correlation between all the parameters again, without this point.

5.4 Comparison with other study sites

5.5.1 Local comparison with Pertuis Charentais salt marshes

CAR averaged values from the estuarine subtidal zone of the Antioche Strait range from 83 +/- 155 to 210 +/- 206 $gC \cdot m^{-2} \cdot y^{-1}$ depending on the time period considered (Table 2). Covering c. 3500 ha, this subtidal zone contributes significantly to the carbon sink function of coastal natural habitats of the region. For comparison with other coastal habitats locally, Amann et al., (2024) reported a mean values for salt marshes from the Pertuis Charentais (Aiguillon, Fier d'Arç and Brouage) of 231 +/- 108 $gC \cdot m^{-2} \cdot y^{-1}$. This means that the rate at which carbon accumulates is similar in salt marshes and the subtidal zone of the Pertuis, for multidecadal periods that are comparable for the two habitats. This work thus contributes to a better understanding of the carbon cycle at the land-ocean interface at national scale (e.g., CarboNium Project, in which this work is framed by; <https://www.pepr-faircarbon.fr/projets/projets-cibles/carbonium>), and contributes locally to support the ambition of the La Rochelle Area towards carbon neutrality by 2040 (LRTZC Project, <https://www.larochelle-zero carbone.fr/nos-actions/travailler-les-puits-de-carbone>).

5.5.2 Global comparison with other subtidal systems

CAR values from this study were then compared with values from other subtidal systems worldwide, reported in the synthesis work by Wilkinson et al. (2018). The comparison shows mean CAR from Antioche that are within the range for most of the sites covered in this synthesis (0 - 250

$gC \cdot m^{-2} \cdot y^{-1}$) (Figure 7). In addition to being relevant compared to the other studies, Antioche Strait is one of the sites with the highest CAR values, with the exception of the extreme values found in the USA and Sweden. In particular, CAR median values from the Antioche are, neglecting 1960-2022 period ($15 gC \cdot m^{-2} \cdot y^{-1}$), respectively 98 and $135 gC \cdot m^{-2} \cdot y^{-1}$ for 1824-2022 and 1824-1960 period are comparable to those found in the Gulf of Finland, with CAR estimated from 28 core samples realized between 2001 and 2004, ranges from 20 to $355 g/m^2/a$ with a median of $114 g/m^2/a$ with higher values found near the coast. In the gulf of Finland, mosaic of hundreds if not thousands of islands, peninsulas and bays, sedimentation rate ($0.5 - 3 cm/a$) were found to be higher near the coast, but TOC (1.3 to 12.6 %) found to be weaker than in deeper water with some distance from it (Vallius, 2015).

However, if sedimentation rates look similar in Antioche Strait, morpho- logical and hydrological settings seem to be different. First of all, the tide is negligible in the Baltic Sea area and supply of particulate matter into the water column comes from Finland watershed, a fluvial input, and from material resuspension in the open sea provoked by wind, wave and sea ice (Vallius, 2015)

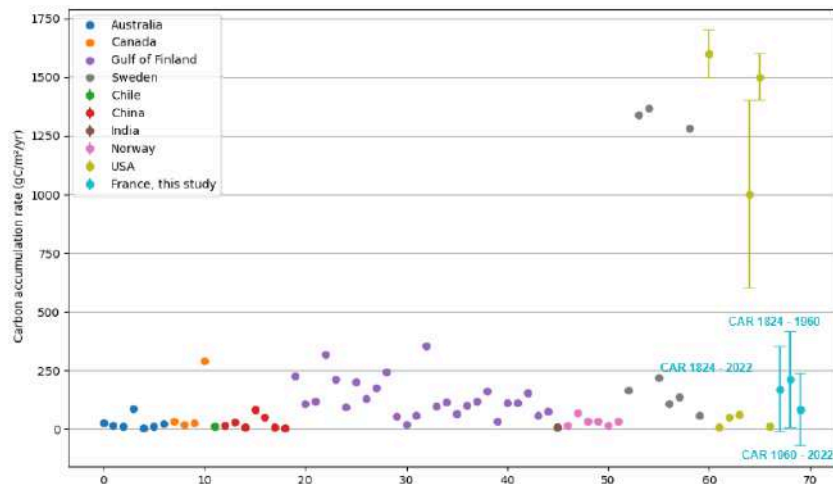


Figure 7: Mean CAR results of the Antioche Strait with its standard deviation, compare to subtidal CAR of continental shelf (Wilkinson et al., 2018)

In our case of open mixed tide and wave estuary, two main differences can be spot from Gulf of Finland study site: (1) TOC values increase the closer you get from the coast in Antioche Strait while it is the opposite in Gulf of Finland, (2) total carbon concentration are find to be higher in the first top centimeter in shallow core of Gulf of Finland, whereas no similar results have been identified in Antioche Strait study. Can these differences be explained only by the tide parameter ?

Conclusion and outlook:

This study provides new insight into the carbon sink potential of subtidal estuarine environments, particularly in the Antioche Strait. It reveals that both sediment accumulation rates (SAR) and total organic carbon content (TOC) strongly govern carbon accumulation (CAR), but also emphasizes the temporal decline in these rates, possibly due to a reduction in free accommodation space and erosion of existing sediment stocks.

One of the most significant implications of the observed recent erosion (1960–2022) is the potential destabilization and release of previously stored carbon, including shallow gas methane formed in anaerobic conditions. This underlines the necessity of integrating these sedimentary carbon reservoirs into regional carbon accounting, particularly within initiatives like the *La Rochelle Territoire Zéro Carbone*.

Future work will improve TOC quantification by performing direct measurements using an elemental analyzer, helping to refine calibration models. Additionally, isotopic carbon analysis ($\delta^{13}C$) will aim to trace the origin (marine vs terrestrial) of the organic matter, while sedimentological studies (e.g.,

grain-size distribution) and hydrodynamic forcing (waves, wind regimes) are recommended to better understand resuspension dynamics. A comparison with other subtidal systems, possibly through a multi-site approach, could help decipher how external forcings impact carbon storage at broader scales. Finally, core analyses from the offshore wind farm project represent a promising extension to deepen spatial understanding and temporal evolution of this coastal carbon sink.

References:

- Amann, B., Chaumillon, E., Schmidt, S., Olivier, L., Jupin, J., Perello, M.C., Walsh, J.P., 2023. Multi-annual and multi-decadal evolution of sediment accretion in a saltmarsh of the French Atlantic coast: Implications for carbon sequestration. *Estuar. Coast. Shelf Sci.* 293, 108467. <https://doi.org/10.1016/j.ecss.2023.108467>
- Amann Benjamin, Chaumillon Eric, Bertin Xavier, Cécilia, P.-M., Perello, M.-C., Dupuy, C., Nathalie, L., Sabine, S., 2024. Understanding sediment and carbon accumulation in macrotidal minerogenic saltmarshes for climate resilience. *Geomorphology* 467, 109465. <https://doi.org/10.1016/j.geomorph.2024.109465>
- Baustian, M.M., Stagg, C.L., Perry, C.L., Moss, L.C., Carruthers, T.J.B., Allison, M., 2017. Relationships Between Salinity and Short-Term Soil Carbon Accumulation Rates from Marsh Types Across a Landscape in the Mississippi River Delta. *Wetlands* 37, 313–324. <https://doi.org/10.1007/s13157-016-0871-3>
- BRGM (direction) (2020). *8.3 Disponibilité des eaux de surface*. Dans *Exploration 70 : Ressources et usages de l'eau en France* (pp. [page–page]). OpenEdition Books. Retrieved June 6, 2025, from : <https://books.openedition.org/pub/663?lang=fr>
- Bertin, X., Chaumillon, E., Sottolichio, A., Pedreros, R., 2005. Tidal inlet response to sediment infilling of the associated bay and possible implications of human activities: the Marennes-Oléron Bay and the Maumusson Inlet, France. *Cont. Shelf Res.* 25, 1115–1131. <https://doi.org/10.1016/j.csr.2004.12.004>
- Breilh, J.-F., Bertin, X., Chaumillon, E., Giloy, N., Sauzeau, T., 2014. How frequent is storm-induced flooding in the central part of the Bay of Biscay? *Glob. Planet. Change* 122, 161–175. <https://doi.org/10.1016/j.gloplacha.2014.08.013>
- Diesing, M., Thorsnes, T., Bjarnadóttir, L.R., 2021. Organic carbon densities and accumulation rates in surface sediments of the North Sea and Skagerrak. *Biogeosciences* 18, 2139–2160. <https://doi.org/10.5194/bg-18-2139-2021>
- García-García, A., Orange, D., Lorenson, T., Radakovitch, O., Tesi, T., Miserocchi, S., Berné, S., Friend, P.L., Nittrouer, C., Normand, A., 2006. Shallow gas off the Rhône prodelta, Gulf of Lions. *Mar. Geol.* 234, 215–231. <https://doi.org/10.1016/j.margeo.2006.09.005>
- Gouleau, D., Jouanneau, J.M., Weber, O., Sauriau, P.G., n.d. Short- and long-term sedimentation on Montportail}Brouage intertidal mud#at, Marennes}Ol Heron Bay (France).
- Laruelle, G.G., Rosentreter, J.A., Regnier, P., 2025. Extrapolation-Based Regionalized Re-evaluation of the Global Estuarine Surface Area. *Estuaries Coasts* 48, 34. <https://doi.org/10.1007/s12237-024-01463-3>
- Macreadie, P.I., Anton, A., Raven, J.A., Beaumont, N., Connolly, R.M., Friess, D.A., Kelleway, J.J., Kennedy, H., Kuwae, T., Lavery, P.S., Lovelock, C.E., Smale, D.A., Apostolaki, E.T., Atwood, T.B., Baldock, J., Bianchi, T.S., Chmura, G.L., Eyre, B.D., Fourqurean, J.W., Hall-Spencer, J.M., Huxham, M., Hendriks, I.E., Krause-Jensen, D., Laffoley, D., Luisetti, T., Marbà, N., Masque, P., McGlathery, K.J., Megonigal, J.P., Murdiyarso, D., Russell, B.D., Santos, R., Serrano, O., Silliman, B.R., Watanabe, K., Duarte, C.M., 2019. The future of Blue Carbon science. *Nat. Commun.* 10, 3998. <https://doi.org/10.1038/s41467-019-11693-w>
- Poirier, C., Chaumillon, E., Arnaud, F., 2011. Siltation of river-influenced coastal environments: Respective impact of late Holocene land use and high-frequency climate changes. *Mar. Geol.* 290, 51–62. <https://doi.org/10.1016/j.margeo.2011.10.008>
- Poirier, C., Sauzeau, T., Chaumillon, E., Tessier, B., 2020. Spatially explicit bathymetric reconstruction from lead line depth soundings of the late 17th century. *Estuar. Coast. Shelf Sci.* 246, 107029. <https://doi.org/10.1016/j.ecss.2020.107029>
- Schmitt, A., Chaumillon, E., 2023. Understanding morphological evolution and sediment dynamics at

- multi-time scales helps balance human activities and protect coastal ecosystems: An example with the Gironde and Pertuis Marine Park. *Sci. Total Environ.* 887, 163819. <https://doi.org/10.1016/j.scitotenv.2023.163819>
- Shom, 2022. MNT topo-bathymétrie côtier des Pertuis Charentais (Projet HOMONIM). https://dx.doi.org/10.17183/MNT_COTIER_PERTUIS_HOMONIM_20m_WGS84
- Toublanc, F., Brenon, I., Coulombier, T., Le Moine, O., 2015. Fortnightly tidal asymmetry inversions and perspectives on sediment dynamics in a macrotidal estuary (Charente, France). *Cont. Shelf Res.* 94, 42–54. <https://doi.org/10.1016/j.csr.2014.12.009>
- Vallius, H., 2015. Sediment and carbon accumulation rates off the southern coast of Finland. *Baltica* 28, 81–88. <https://doi.org/10.5200/baltica.2015.28.08>
- Weber, N., Chaumillon, E., n.d. Long term evolution of sandwaves in estuaries illustrated by active, intermediate and moribund sandwaves of the French Atlantic coast (Charente-maritime).
- Weber, N., Chaumillon, E., Tesson, M., Garlan, T., 2004. Architecture and morphology of the outer segment of a mixed tide and wave-dominated-incised valley, revealed by HR seismic reflection profiling: the paleo-Charente River, France. *Mar. Geol.* 207, 17–38. <https://doi.org/10.1016/j.margeo.2004.04.001>
- Wilkinson, G.M., Besterman, A., Buelo, C., Gephart, J., Pace, M.L., 2018. A synthesis of modern organic carbon accumulation rates in coastal and aquatic inland ecosystems. *Sci. Rep.* 8, 15736. <https://doi.org/10.1038/s41598-018-34126-y>

Supplementary resources:

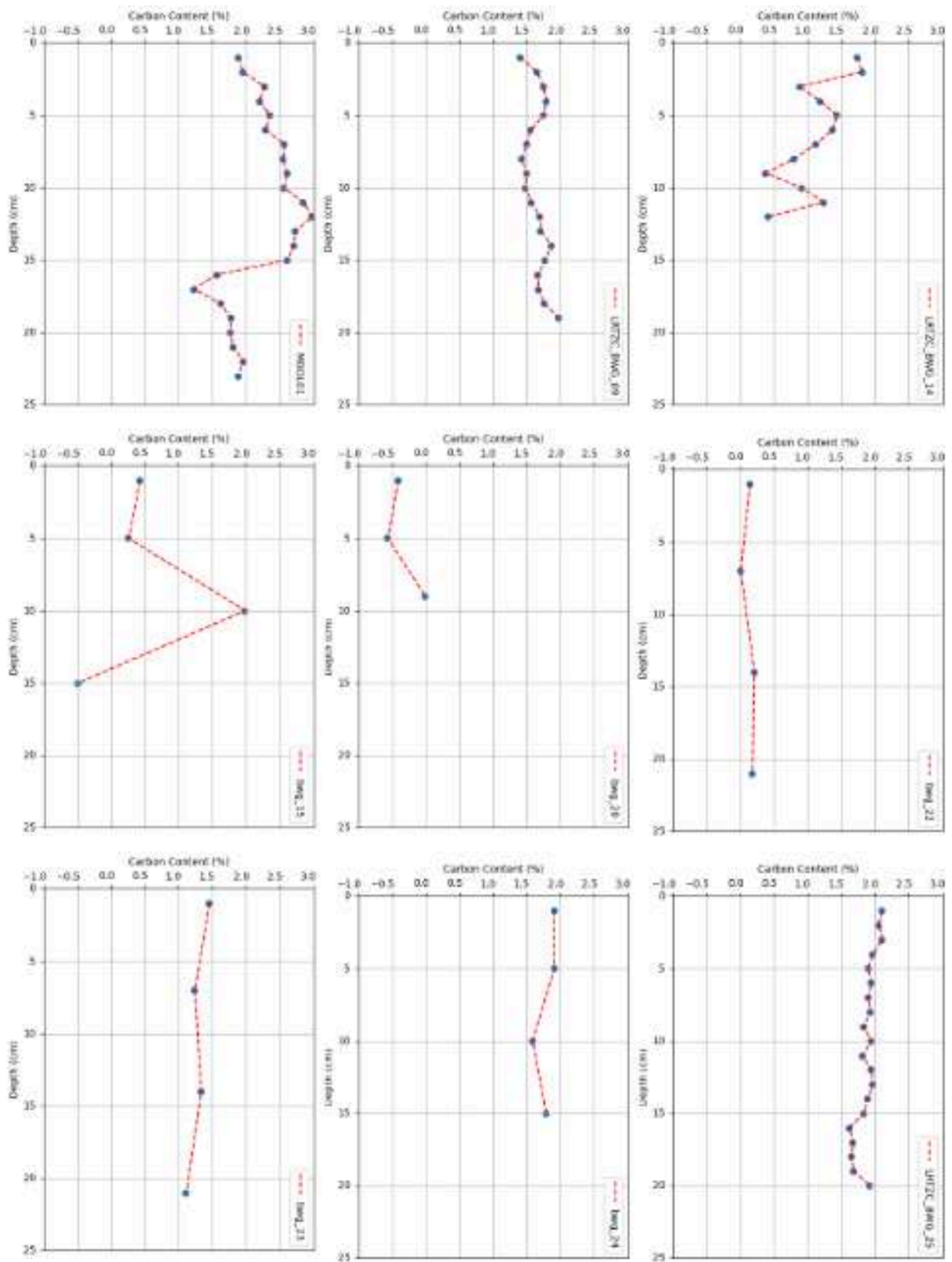
Appendix 1: Description of the core and grab sampled retrieved during the Campagne à la mer course.

Hour	Sample_ID	Long93	Lat93	sediment description	Profondeur_eau (m)	Sampl e_tool	theoretical_core_s ize (cm)	real_core_size (cm)
9:06:00 AM	mggl_03	390560,59	6552313,16	Sable vaseux avec galets	15.3	grab		NA
9:22:00 AM	mggl_02	390560,59	6552313,16	Vase	23	grab		NA
9:38:00 AM	mggl_02	390560,59	6552313,16		22.7	core	31.5	27
10:08:00 AM	mggl_01	390560,59	6552313,16	Vase	21.3	grab		NA
10:19:00 AM	mggl_01	390560,59	6552313,16		21.6	core	26	23
11:48:00 AM	lrtzc_bwg24_03	390560,59	6552313,16	Vase	18	grab		NA
1:05:00 PM	lrtzc_bwg24_03	390560,59	6552313,16		18.5	core	15	15
1:21:00 PM	lrtzc_bwg24_04	390560,59	6552313,16	Sable vaseux	11.3	grab		NA
1:36:00 PM	lrtzc_bwg24_09	390560,59	6552313,16	Vase	21.2	grab		NA
1:50:00 PM	lrtzc_bwg24_09?	390560,59	6552313,16		19.9	core	16	17
2:00:00 PM	lrtzc_bwg24_15	390560,59	6552313,16	Vase	24.9	grab		NA
2:12:00 PM	lrtzc_bwg24_15	390560,59	6552313,16		24.5	core	20	17
2:26:00 PM	lrtzc_bwg24_14	390560,59	6552313,16	Vase fine	34.8	grab		NA
2:47:00 PM	lrtzc_bwg24_14	390560,59	6552313,16		31.8	core	15	12
3:03:00 PM	lrtzc_bwg24_13	390560,59	6552313,16	Sable vaseux	28.2	grab		NA
3:07:00 PM	lrtzc_bwg24_13	390560,59	6552313,16		28	core	10	8
15.24	lrtzc_bwg24_20	390560,59	6552313,16	Sable vaseux	31.9	grab		NA
3:32:00 PM	lrtzc_bwg24_20	390560,59	6552313,16		30.5	core	15	9
9:48:00 AM	LRTCZ_BW G24_25	390560,59	6552313,16	Niveau de sable a 10 a 14cm	19	core	20	20
10:23:00 AM	LRTCZ_BW G24_24	390560,59	6552313,16	Niveau de sable a 10 a 14cm	14.5	core		15
1:10:00 PM	LRTCZ_BW G24_23	390560,59	6552313,16		13.7	core	26.5	24
1:55:00 PM	LRTCZ_BW G24_22	390560,59	6552313,16		14.6	core	30	25

2:19:00 PM	LRTCZ_BW G24_20	390560,59	6552313,16	Carottage infructueux (Sable et Coquillages)	27.4	core	-	NA
2:41:00 PM	MGGL_05	390560,59	6552313,16		24.4	core	24.5	23
3:04:00 PM	MGGL_04	390560,59	6552313,16	Sableux	24.1	core	5	4
3:20:00 PM	LRTCZ_BW G24_09	390560,59	6552313,16		22	core		19

Appendix 2: Carbon content profile over the depth (A), water content (B) for the nine core samples studied. From left to right and top to bottom following the north south gradient used before

A



B

